Int. J. Heat Mass Transfer. Vol. 32, No. 7, pp. 1309–1319, 1989
Printed in Great Britain

0017-9310/89 \$3.00+0.00

Mixed convection over rotating bodies with blowing and suction

TIAN-YIH WANG and CLEMENT KLEINSTREUER†
Department of Mechanical and Aerospace Engineering, North Carolina State University, Raleigh, NC 27695-7910, U.S.A.

(*Received* 11 *August* 1988 *and in final form* 29 *November* 1988)

Abstract—The non-similar boundary-layer analysis of steady laminar mixed convection heat transfer from an axisymmetric body is extended and unified. Velocity profiles and temperature distributions in the attached boundary layers are studied for the entire range from pure forced convection to pure free convection. The validated computer simulation model is successfully applied to the case of mixed thermal convection of arbitrary Prandtl number fluids past a sphere with optional body rotation, fluid suction or injection, surface heating or cooling mode, and isothermal or constant-flux wall condition.

1. INTRODUCTION

NUMEROUS industrial applications involve both forced and natural convection along axisymmetric bodies where special effects such as body rotation, surface mass transfer, the heating/cooling mode, and the type of thermal wall condition are important. Examples include rotary machine design, transpiration cooling, projectile behavior, and wire or fiber coating. Spin motion enhances convection heat transfer when the centrifugal force pushes the near-surface fluid outwards which is being replaced by cooler or warmer fluid depending upon the wall temperature. Momentum and heat transfer rates may also be affected by the buoyancy force which assists the forced flow for heated surfaces and retards in the case of cooled surfaces when the fluid is moving upwards against the gravitational force. For porous or perforated submerged bodies, mass transfer at the wall, in terms of fluid injection or withdrawal at a prescribed temperature, can alter the local skin friction coefficient and the local Nusselt number significantly.

Previous studies concentrated on some or all of these special effects including the influence of power-law fluids on fluid mechanics and heat transfer parameters. However, these analyses are valid only for forced- *or* free-convection dominated regimes [1–5]. In contrast, mixed convection parameters which cover the entire range from pure forced to pure free convection heat transfer have only been very recently developed for thermal flow past vertical flat plates [6] and slender cylinders [7, 8]. Tien and Tsuji [1] investigated thermal flow over a rotating disk. Chao and Greif [2] assumed a quadratic velocity profile to study forced convection heat transfer along rotating bodies with arbitrary surface temperature. Lee *et al.* [3] analyzed the momentum and heat transfer rates through laminar boundary layers over rotating isothermal bodies by employing Merk's series expansion technique. Lien *et al.* [4] introduced two sets of transformation variables to simulate mixed convection and pure free convection around a sphere, separately. They assumed the potential flow solution as the outer velocity distribution. Reference [5] used an implicit finite difference method to solve the problem of mixed thermal convection of rotating porous bodies placed in power-law fluids. Lin and Chen [6] proposed a new mixed convection parameter for steady laminar flow past a vertical isothermal plate covering the entire range of convection heat transfer. Lee *et al.* [7] analyzed mixed convection along a vertical slender cylinder with transformation parameters which also allow a simulation of the full transition from pure forced to pure free convection. Reference [8] advanced the previous contributions [6, 7] and developed two uniquely transformed sets of axisymmetric boundary-layer equations for the constant wall heat flux case and the isothermal surface case. These equations have been solved, using Keller's box method, without numerical problems (i.e. 'stiff' differential equations) or parametric restrictions (i.e. $Pr \leqslant 100$) as reported by Lee *et al.* [7].

The general analysis developed and discussed in this paper is an extension of the work of ref. [8] and contains the previous contributions [1–4] as distinct special cases.

2. ANALYSIS

Figure 1 depicts axisymmetric boundary-layer past a spinning permeable body placed in a uniform stream moving opposite to the gravitational force and parallel to the axis of body rotation. Considering steady laminar flow, the describing equations, boundary conditions and suitable coordinate transformations are developed for two distinct thermal boundary con-

† Author to whom all correspondence should be addressed.

NOMENCLATURE

BP	rotation parameter, $(L^2\Omega/(\nu\lambda^2))^2$
BP^*	rotation parameter, $4/9(R\Omega/u_\infty)^2$
BP^{**}	rotation parameter, $(\pi R\Omega/(2u_\infty))^2$
c_f	local skin friction coefficient
F	dimensionless stream function
G	dimensionless velocity
Gr	Grashof number (T_w = const.)
Gr^*	Grashof number (q_w = const.)
g	gravitational acceleration
h	local heat transfer coefficient
k	thermal conductivity
L	characteristic length of axisymmetric body
MP	mass transfer parameter
Nu	local Nusselt number
Nu^*	local Nusselt number (rotating disk case)
Pr	Prandtl number
q	local heat transfer rate
R	radius of sphere
Ra	Rayleigh number (isothermal wall case)
Ra^*	Rayleigh number (constant wall heat flux case)
Re	Reynolds number
Re_x^*	Reynolds number (rotating disk case)
r	distance from a point on the surface to the axis of symmetry
T	temperature
U	pseudo-velocity
u	velocity component in the x-direction
v	velocity component in the y-direction
w	transverse velocity component
x	streamwise coordinate along the body surface measured from the forward stagnation point
y	coordinate normal to the surface
Z	dimensionless parameter; 1 for heated and -1 for cooled submerged body.

Greek symbols

α	thermal diffusivity
β	thermal expansion coefficient
γ	dimensionless parameter
ζ	mixed convection parameter (T_w = const.)
ζ^*	mixed convection parameter (q_w = const.)
η	dimensionless coordinate
η^*	dimensionless coordinate, $Re^{1/2}y/R$
θ	dimensionless temperature
λ	dimensionless buoyancy parameter
ν	kinematic viscosity
ξ	dimensionless coordinate
ρ	density of fluid
σ	dimensionless parameter
τ	shear stress
ϕ	angle between the gravitational acceleration vector and the outward normal to the body force
ψ	stream function
Ω	angular velocity.

Subscripts

e	boundary layer edge condition
q	constant wall heat flux case
T	constant wall temperature case
w	wall condition
∞	ambient conditions.

ditions, i.e. constant wall heat flux and isothermal surface. In either case, the wall temperature may be higher than the ambient (heating mode; $Z = 1$) or lower (cooling mode; $Z = -1$). The fluid properties are considered to be constant except for temperature-induced density variations in the body-force term.

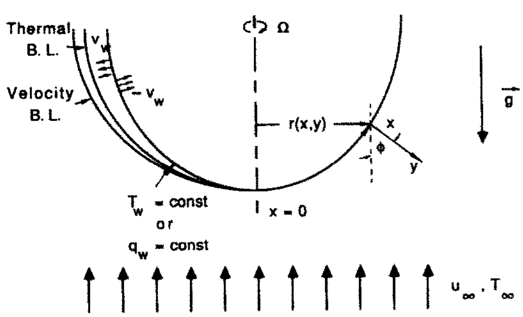

FIG. 1. System schematics and coordinates.

Wake effects on the attached boundary layer are neglected. The general analysis is then applied to the case of a rotating, permeable sphere.

2.1. *The governing equations and transformation parameters*

Non-rotating coordinates are chosen where x is the distance from the forward stagnation point along a meridian curve and y is measured normal to the body surface (Fig. 1). With the stated assumptions and the Boussinesq approximation, the governing equations are

$$\frac{\partial}{\partial x}(ru)+\frac{\partial}{\partial y}(rv)=0 \tag{1}$$

$$u\frac{\partial u}{\partial x}+v\frac{\partial u}{\partial y}-\frac{w^2}{r}\frac{\mathrm{d}r}{\mathrm{d}x}=u_e\frac{\mathrm{d}u_e}{\mathrm{d}x} + Zg\beta|T-T_\infty|\sin\phi+\nu\frac{\partial^2 u}{\partial y^2} \tag{2}$$

$$u\frac{\partial w}{\partial x}+v\frac{\partial w}{\partial y}+\frac{uw}{r}\frac{\mathrm{d}r}{\mathrm{d}x}=v\frac{\partial^2 w}{\mathrm{d}y^2} \tag{3}$$

$$u\frac{\partial T}{\partial x}+v\frac{\partial T}{\partial y}=\alpha\frac{\partial^2 T}{\mathrm{d}y^2}. \tag{4}$$

The associated boundary conditions are

$$\text{at } y\to\infty:\quad u=u_e(x),\quad w=0\quad\text{and}\quad T=T_\infty \tag{5}$$

at $y=0$:

$$u=0,\quad v=\pm v_w,\quad w=r\Omega\quad\text{and}\quad T=T_w=\text{const.} \tag{6a}$$

or

at $y=0$:

$$u=0,\quad v=\pm v_w,\quad w=r\Omega$$

$$\text{and}\quad q=-k\frac{\partial T}{\partial y}=\text{const.} \tag{6b}$$

In order to facilitate the numerical solution, the x-dependence of certain terms in the governing equations is reduced and the boundary conditions are simplified. This is accomplished with coordinate transformations for the isothermal wall and constant flux cases based on a proper choice of transformation parameters derived from scale analysis (cf. ref. [9]). The dimensionless parameters are

$$\xi=x/L;\quad \eta=\lambda\xi^{-1/2}(u_e/u_\infty)^{1/2}y/L \tag{7a,b}$$

$$\psi=r\alpha\lambda\xi^{1/2}\left(\frac{u_e}{u_\infty}\right)^{1/2}F(\xi,\eta)-\int_0^x rv_w\,\mathrm{d}x;\quad G=\frac{w}{r\Omega} \tag{8a,b}$$

$$\theta=\begin{cases}\dfrac{T-T_\infty}{T_w-T_\infty} & \text{for } T_w=\text{const.}\\[2ex] \dfrac{T-T_\infty}{(q_wL/k\lambda)\xi^{1/2}(u_\infty/u_e)^{1/2}} & \text{for } q_w=\text{const.}\end{cases} \tag{9a,b}$$

The dimensionless buoyancy parameter λ is defined as

$$\lambda=\begin{cases}(\gamma Re)^{1/2}+(\sigma Ra)^{1/4}=(\gamma Re)^{1/2}/(1-\zeta)\\ \qquad=(\sigma Ra)^{1/4}/\zeta\quad\text{for}\quad T_w=\text{const.}\\ (\gamma Re)^{1/2}+(\sigma Ra^*)^{1/5}=(\gamma Re)^{1/2}/(1-\zeta^*)\\ \qquad=(\sigma Ra^*)^{1/5}/\zeta\quad\text{for}\quad q_w=\text{const.}\end{cases} \tag{10a,b}$$

where

$$Re=u_\infty L/v,\quad Ra=g\beta|T_w-T_\infty|L^3/(\alpha v),$$
$$Ra^*=g\beta|q_w|L^4/(\alpha vk) \tag{11a–c}$$

$$\gamma=Pr/(1+Pr)^{1/3}\quad\text{and}\quad\sigma=Pr/(1+Pr). \tag{12a,b}$$

The mixed convection parameters ζ for $T_w=$ const. and ζ^* for $q_w=$ const., covering the entire range from pure forced to pure free convection, are defined as

$$\zeta=(\sigma Ra)^{1/4}/[(\gamma Re)^{1/2}+(\sigma Ra)^{1/4}] \tag{13a}$$

and

$$\zeta^*=(\sigma Ra^*)^{1/5}/[(\gamma Re)^{1/2}+(\sigma Ra^*)^{1/5}]. \tag{13b}$$

For large Prandtl number fluids, ξ reduces to $Ra^{1/4}/(Re^{1/2}\ Pr^{1/3})$ and ζ^* simplifies to $Ra^{*1/5}/(Re^{1/2}Pr^{1/3})$ while for small Prandtl number, $\zeta\to(Ra\,Pr)^{1/4}/(Re\,Pr)^{1/2}$ and $\zeta^*\to(Ra^*Pr)^{1/5}/(Re\,Pr)^{1/2}$ as known from scale analysis.

Using the stream function approach

$$u=\frac{1}{r}\frac{\partial\psi}{\partial y}\quad\text{and}\quad v=-\frac{1}{r}\frac{\partial\psi}{\partial x} \tag{14a,b}$$

the continuity equation is automatically satisfied and two sets of transformed equations in $F(\xi,\eta)$, $G(\xi,\eta)$ and $\theta(\xi,\eta)$ can be derived for the two thermal boundary conditions.

2.2. *The transformed equations for the isothermal wall case*

Substituting equations (7)–(9a) into equations (2)–(6) yields

$$Pr\,F'''+B(\xi)FF''-A(\xi)F'^2+C(\xi,\zeta)$$
$$+E(\xi)G^2+MP\,D(\xi)F''+ZS(\xi,\zeta)\theta$$
$$=\xi\left[F'\frac{\partial F'}{\partial\xi}-F''\frac{\partial F}{\partial\xi}\right] \tag{15}$$

$$Pr\,G''+B(\xi)FG'-H(\xi)GF'-MP\,D(\xi)G'$$
$$=\xi\left[F'\frac{\partial G}{\partial\xi}G'\frac{\partial F}{\partial\xi}\right] \tag{16}$$

and

$$\theta''+B(\xi)F\theta'-MP\,D(\xi)\theta'=\xi\left[F'\frac{\partial\theta}{\partial\xi}-\theta'\frac{\partial F}{\partial\xi}\right]. \tag{17}$$

The associated boundary conditions are

$$F(\xi,0)=F'(\xi,0)=0;\quad G(\xi,0)=1$$
$$\text{and}\quad\theta(\xi,0)=1 \tag{18}$$

$$F'(\xi,\infty)=(1+Pr)^{1/3}(1-\zeta)^2;\quad G(\xi,\infty)=0$$
$$\text{and}\quad\theta(\xi,\infty)=0. \tag{19}$$

The primes denote differentiation with respect to η. The system parameters of special interest include

$$BP=\left(\frac{L^2\Omega}{v\lambda^2}\right)^2\quad\text{and}\quad MP=\pm\frac{v_wL}{\alpha\lambda}. \tag{20a,b}$$

The coefficients in equations (15)–(17) are defined as

$$A(\xi)=(\xi/u_e)(\mathrm{d}u_e/\mathrm{d}\xi) \tag{21a}$$

$$B(\xi)=(\xi/r)(\mathrm{d}r/\mathrm{d}\xi)+(1+A(\xi))/2 \tag{21b}$$

$$C(\xi,\zeta) = (1+Pr)^{2/3}(1-\zeta)^4 A(\zeta) \quad (21c)$$

$$D(\xi) = \xi^{1/2}/(u_e/u_\infty)^{1/2} \quad (21d)$$

$$E(\xi) = Pr^2 BP(\xi/r)(dr/d\xi)((r/L)/(u_e/u_\infty))^2 \quad (21e)$$

$$H(\xi) = 2(\xi/r)(dr/d\xi) \quad (21f)$$

$$S(\xi,\zeta) = (1+Pr)\zeta^4\xi \sin\xi/(u_e/u_\infty)^2. \quad (21g)$$

The physical quantities of primary interest are the local skin friction coefficient c_f and the local Nusselt number Nu. In order to deal with the whole region of mixed convection, we defined the local skin friction coefficient as

$$c_f = \tau_w/(1/2\rho U^2) \quad (22)$$

where U is a pseudo or reference velocity defined here as

$$U_T = u_\infty + [g\beta|T_w - T_\infty|L]^{1/2}. \quad (23)$$

Hence a dimensionless skin friction parameter can be formed as

$$SFP_T = \frac{1}{2}c_f\lambda = \frac{F''(\xi,0)}{Pr}\xi^{-1/2}(u_e/u_\infty)^{3/2} \times [(1-\zeta)^2/\gamma + \zeta^2/(\sigma Pr)^{1/2}]^{-2} \quad (24)$$

whereas the traditional SFG, restricted to $0 \leqslant \zeta < 1$, is given as

$$SFG = \tfrac{1}{2}c_f Re^{1/2} = F''(\xi,0)\xi^{-1/2}(u_e/u_\infty)^{3/2}\sigma^{1/2}/(1-\zeta)^3. \quad (25)$$

Similarly, with the definition of the local Nusselt number

$$Nu = hL/k \quad (26)$$

a dimensionless heat transfer parameter for the isothermal wall case can be formed as

$$HTP_T = Nu/\lambda = -\xi^{-1/2}(u_e/u_\infty)^{1/2}\theta'(\xi,0). \quad (27a)$$

This is in contrast to the traditional definition of the heat transfer group for a forced-flow dominated regime ($0 \leqslant \zeta < 1$)

$$HTG_T = Nu/Re^{1/2} = -\gamma^{1/2}\xi^{-1/2}(u_e/u_\infty)^{1/2}\theta'(\xi,0)/(1-\zeta) \quad (27b)$$

and for the buoyancy-flow dominated regime ($0 < \zeta \leqslant 1$)

$$HTG_T = Nu/Gr^{1/4} = -(Pr\,\sigma)^{1/4}\xi^{-1/2}(u_e/u_\infty)^{1/2}\theta'(\xi,0)/\zeta. \quad (27c)$$

In order to solve a specific problem, the shape of the body $r(x)$, its characteristic length L, and the outer flow distribution $(u_e(x)/u_\infty)$ have to be known.

2.3. *The transformed equations for the constant wall heat flux case*

The uniquely transformed temperature (equation (9b)) for the thermal boundary condition $q_w =$ const. causes slight changes in the transformed equations and boundary conditions when compared with the isothermal wall case. Here, equations (2)–(4) are transformed to

$$Pr\,F''' + B(\xi)FF'' - A(\xi)F'^2 + C^*(\xi,\zeta^*) + E(\xi)G^2 - MP\,D(\xi)F'' + ZS^*(\xi,\zeta^*)\theta = \xi\left[F'\frac{\partial F'}{\partial\xi} - F''\frac{\partial F}{\partial\xi}\right] \quad (28)$$

$$Pr\,G'' + B(\xi)FG' - H(\xi)GF' - MP\,D(\xi)G' = \xi\left[F'\frac{\partial G}{\partial\xi} - G'\frac{\partial F}{\partial\xi}\right] \quad (29)$$

and

$$\theta'' + B(\xi)F\theta' - N(\xi)F'\theta - MP\,D(\xi)\theta' = \xi\left[F'\frac{\partial\theta}{\partial\xi} - \theta'\frac{\partial F}{\partial\xi}\right]. \quad (30)$$

The corresponding boundary conditions are

$$F(\xi,0) = F'(\xi,0) = 0, \quad G(\xi,0) = 1 \quad \text{and} \quad \theta'(\xi,0) = -1 \quad (31)$$

$$F'(\xi,\infty) = (1+Pr)^{1/3}(1-\zeta^*)^2, \quad G(\xi,\infty) = 0. \quad \text{and} \quad \theta(\xi,\infty) = 0. \quad (32)$$

The new coefficients in equations (28)–(30) are

$$C^*(\xi,\zeta^*) = (1+Pr)^{2/3}(1-\zeta^*)^4 A(\xi) \quad (33a)$$

$$N(\xi) = 1/2(1-A(\xi)) \quad (33b)$$

and

$$S^*(\xi,\zeta^*) = (1+Pr)\zeta^{*5}\xi^{3/2}\sin\xi/(u_e/u_\infty)^{5/2}. \quad (33c)$$

The dimensionless heat transfer parameter, HTP_q, is now defined as

$$HTP_q = Nu/\lambda = \xi^{-1/2}(u_e/u_\infty)^{1/2}/\theta(\xi,0). \quad (34a)$$

Thus, for $0 \leqslant \zeta^* < 1$

$$HTG_q = Nu/Re^{1/2} = \gamma^{1/2}\xi^{-1/2}(u_e/u_\infty)^{1/2}/((1-\zeta^*)\theta(\xi,0)) \quad (34b)$$

and for $0 < \zeta^* \leqslant 1$

$$HTG_q = Nu/Gr^{*1/5} = (Pr\,\sigma)^{1/5}\xi^{-1/2}(u_e/u_\infty)^{1/2}/(\zeta^*\theta(\xi,0)). \quad (34c)$$

Using a pseudo-velocity defined as

$$U_q = u_\infty + [g\beta|q_w|L^{3/2}\nu^{1/2}/k]^{2/5} \quad (35)$$

a dimensionless skin friction parameter for the constant wall heat flux case can be formed as

$$SFP_q = \frac{1}{2}c_f\lambda = \frac{F''(\xi,0)}{Pr}\xi^{-1/2}(u_e/u_\infty)^{3/2} \times [(1-\zeta^*)^2/\gamma + \zeta^{*2}/(\sigma Pr)^{2/5}]^{-2} \quad (36a)$$

where the traditional SFG, restricted to $0 \leqslant \zeta^* < 1$, is given as

$$SFG = \frac{1}{2} c_f \, Re^{1/2}$$

$$= F''(\xi, 0)\xi^{-1/2}(u_e/u_\infty)^{3/2}\sigma^{1/2}/(1-\zeta^*)^3. \quad (36b)$$

All other parameters are the same as given in Section 2.2.

2.4 *Applications to a rotating permeable sphere*

For a sphere, $r(x) = R \sin(x/R)$ and $\phi = x/R \equiv \xi$, where R is the radius of the sphere which corresponds to the characteristic length L. Two different edge velocity distributions may be used to carry out the calculations. One is the potential flow

$$u_e/u_\infty = 3/2 \sin(x/R), \quad x > 0 \quad (37)$$

and the other one is based on measurements performed by Frössling as given in White [10]

$$u_e/u_\infty = 1.5\xi - 0.4371\xi^3 + 0.1481\xi^5 - 0.0423\xi^7, \quad \xi > 0. \quad (38)$$

Equation (37) has been used for comparison purposes with previously published results. However, equation (38) is assumed here for all other computations since it describes the outer flow more realistically. The expression of Frössling is valid for $x/R \leqslant 1.48$. Thus, the results presented are terminated at $\phi = 90°$.

3. NUMERICAL SOLUTION

The transformation of the governing equations reduces the numerical work significantly. The resulting system of coupled equations with the appropriate coefficients for the two thermal boundary conditions were solved with a two-point finite difference method outlined by Cebeci and Bradshaw [11].

The two-dimensional grid is nonuniform in order to accommodate the steep velocity and temperature gradients at the wall, particularly in the vicinity of the singular point at $\xi = 0$. The location of the boundary-layer edge, η_∞, depends strongly on the fluid Prandtl number, Pr, and the magnitude of the mixed convection parameters, ζ and ξ^*. For example, η_∞ ($Pr = 0.001$, $\zeta = 0.0$ and $BP = 0.0$) ≈ 6 and η_∞ ($Pr = 10^4$, $\zeta = 1.0$ and $BP = 0.0$) ≈ 800. The latter case almost violates the thin shear layer assumption. The independence of the results from the mesh density has been successfully tested.

4. RESULTS AND DISCUSSION

The numerical computations were carried out for the entire range of mixed thermal convection considering both forced-flow assisting and forced-flow opposing modes for two different thermal wall con-

Table 1. Comparison of skin friction coefficient and Nusselt number for forced flow against a rotating disk; $\zeta = 0$, $MP = 0$, $Z = 1$

BP^{**}	$c_f Re_x^{*1/2}$			Nu^*							
				$Pr = 1.0$				$Pr = 10$			
	Present method	Lee *et al.* (1978)	Tifford and Chu (1952)	Present method	Lee *et al.* (1978)	Tien and Tsuji (1964)	Chao and Greif (1974)	Present method	Lee *et al.* (1978)	Tien and Tsuji (1964)	Chao and Greif (1974)
0	2.6237	2.6239	2.61	0.7621	—	0.762	0.7594	1.7510	—	1.752	1.752
1	1.8717	1.8717	1.83	0.6582	0.6583	0.658	0.6113	1.5345	1.5354	1.535	1.518
4	1.3732	1.3734	1.38	0.5576	0.5577	0.557	0.432	1.3403	1.3410	1.340	1.297

Table 2(a). Comparison of $1/2c_f Re^{1/2}$ for forced convection past a rotating sphere; $\zeta = 0$, $MP = 0$, $Z = 1$

	$BP^* = 1$			$BP^* = 4$		
ξ	Present method	Lien *et al.* (1986)	Lee *et al.* (1978)	Present method	Lien *et al.* (1986)	Lee *et al.* (1978)
0.474	1.2499	1.2499	1.2496	1.8174	1.8182	1.8170
0.951	1.8400	1.8400	1.8403	2.6356	2.6360	2.6362
1.215	1.7184	1.7185	1.7207	2.3979	2.3990	2.4032
1.374	1.4727	1.4732	1.4780	1.9769	1.9786	1.9892
1.486	1.2171	1.2173	1.2269	1.5361	1.5373	1.5644

Table 2(b). Comparison of $Nu\, Re^{-1/2}$ for forced convection past a rotating sphere; $Pr = 1$, $\zeta = 0$, $MP = 0$, $Z = 1$

	$BP^* = 1$			$BP^* = 4$		
ξ	Present method	Lien *et al.* (1986)	Lee *et al.* (1978)	Present method	Lien *et al.* (1986)	Lee *et al.* (1978)
0.0	0.9587	0.9586	0.9588	1.0213	1.0213	1.0214
0.951	0.7994	0.7993	0.7998	0.8480	0.8480	0.8484
1.215	0.6965	0.6966	0.6961	0.7338	0.7339	0.7328
1.374	0.6194	0.6195	0.6171	0.6455	0.6459	0.6414
1.486	0.5556	0.5559	0.5510	0.5692	0.5698	0.5593

ditions. Of special interest are the effects of fluid Prandtl number as well as body rotation and wall mass transfer on the local skin friction coefficient and the local Nusselt number. Before the results of the parametric sensitivity analyses are shown, the accuracy of the present computer simulation model is examined.

4.1. *Data comparisons for special case studies*

The first case study is forced convection heat transfer of an isothermal rotating disk (Table 1). Here, $r = x$, $L = R$, $u_e/u_\infty = 2x/\pi R$, $BP^{**} = (\pi R\Omega/2u_\infty)^2$, and $Re_x^* = (M^2+\Omega^2)^{1/2}x^2/\nu$ where $M = 2u_\infty/\pi R$. The relevant system parameters are defined as $c_f = \tau_w/[1/2\rho(M^2+\Omega^2)x^2]$ and $Nu^* = q_w \nu^{1/2}/[k(T_w-T_\infty)(M^2+\Omega^2)^{1/4}]$. The average skin friction values and Nusselt numbers compare very well with previously published data sets for all rotation parameters and Prandtl number fluids considered (Table 1).

The second case study deals with an isothermal rotating sphere considering pure forced convection (Tables 2(a) and (b)) and pure free convection (Table 3). Tables 2(a) and (b) show, respectively, a com-

Table 3. Comparison of wall shear stress distribution and local Nusselt numbers for natural convection from an isothermal rotating sphere; $Pr = 0.7$, $\zeta = 1.0$, $MP = 0$, $Z = 1$

		$\tau_w/(\rho(\nu/R)^2 Gr^{3/4})$		$Nu\, Gr^{-1/4}$	
BP^*	ϕ	Lien *et al.* (1986)	Present method	Lien *et al.* (1986)	Present method
	0	—	0.0	0.4869	0.4869
	10	0.1867	0.1867	—	0.4854
1	30	0.5304	0.5304	0.4732	0.4733
	60	0.8799	0.8799	0.4326	0.4327
	90	0.9472	0.9471	0.3649	0.3651
	0	—	0.0	0.5502	0.5501
	10	0.3246	0.3244	—	0.5478
4	30	0.8961	0.8955	0.5294	0.5293
	60	1.3201	1.3192	0.4671	0.4670
	90	1.0101	1.0089	0.3575	0.3574
	0		0.0	0.6324	0.6319
	10	0.5500	0.5554	—	0.6288
10	30	1.5141	1.5124	0.6044	0.6040
	60	2.0875	2.0848	0.5190	0.5186
	90	1.1302	1.1254	0.3539	0.3529

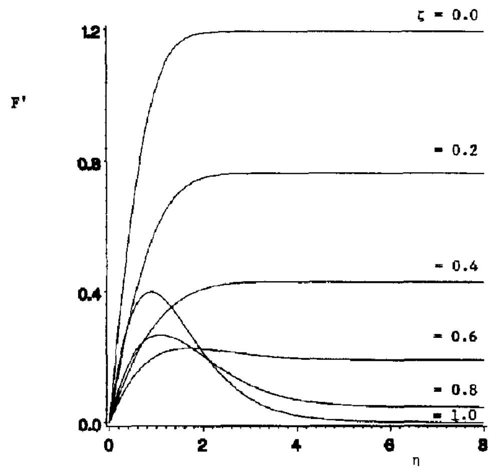

FIG. 2. $F'(\eta)$-profiles at $\phi = 60°$ on a heated isothermal sphere for entire free–forced convection range ($Z = 1$, $Pr = 0.7$, $BP = 1$, $MP = 0$).

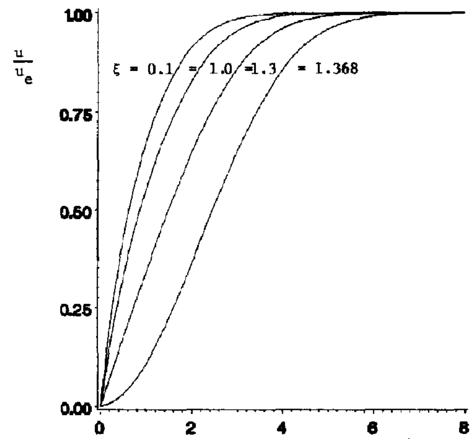

FIG. 4. Streamwise velocity profiles at various locations for a cooled isothermal sphere ($Z = -1$, $Pr = 0.7$, $\zeta = 0.5$, $BP = 1$, $MP = 0$).

parison of local skin friction values and local Nusselt numbers with literature data for two angular velocities where $BP^* = 4/9(R\Omega/u_\infty)^2$. In Table 3, a good agreement is documented for the wall shear stress distribution and the local Nusselt numbers when $BP^* = 1, 4$ and 10. For $BP = 0$ and $MP = 0$, the local heat transfer parameter for a combined free–forced convection case has been compared with $(Nu/Re^{1/2})$ data obtained by Chen and Mucoglu [12] as shown in Fig. 10(b).

4.2. *Representative velocity and temperature profiles around a sphere*

Depending upon the thermal wall condition, the dimensionless profile $F'(\xi, \eta)$ is related to the streamwise velocity $u(x, y)$ as (cf. Section 2.1)

$$(u/u_e)_T = F'(\xi,\eta)/[(1+Pr)^{1/3}(1-\zeta)^2] \quad \text{for } T_w = \text{const.} \tag{39a}$$

and

$$(u/u_e)_q = F'(\xi,\eta)/[(1+Pr)^{1/3}(1-\zeta^*)^2] \quad \text{for } q_w = \text{const.} \tag{39b}$$

for the forced-convection dominated case, i.e. $0 \leqslant \zeta$ or $\zeta^* < 1$ and for the free-convection dominated case, i.e. $0 < \zeta$ or $\zeta^* \leqslant 1$

$$u/[(\alpha/R)Ra^{1/2}] = \sigma^{1/2}F'(\xi,\eta)(u_e/u_\infty)/\zeta^2 \quad \text{for } T_w = \text{const.} \tag{40a}$$

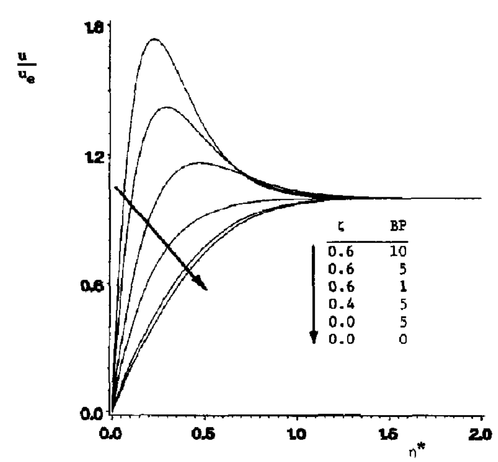

FIG. 3. Streamwise velocity profiles at $\phi = 60°$ for mixed convection past a heated rotating sphere ($Z = 1$, $Pr = 0.7$, $MP = 0$).

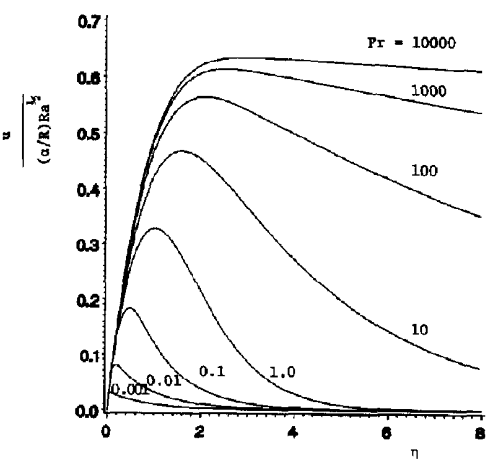

FIG. 5. Prandtl number effect on the velocity at $\phi = 60°$ for natural convection from a heated isothermal sphere ($Z = 1$, $BP = MP = 0$, $\zeta = 1$).

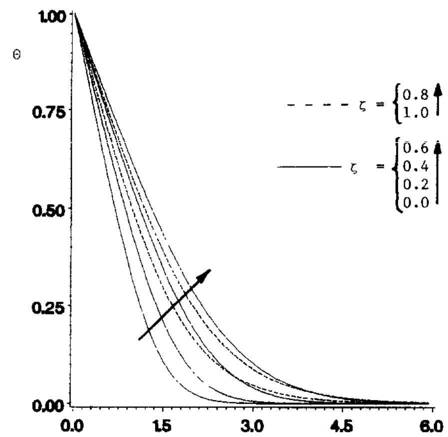

FIG. 6. Representative temperature profiles at $\phi = 60^\circ$ on a heated sphere for entire free–forced convection range ($Pr = 0.7$, $BP = 1$, $MP = 0$).

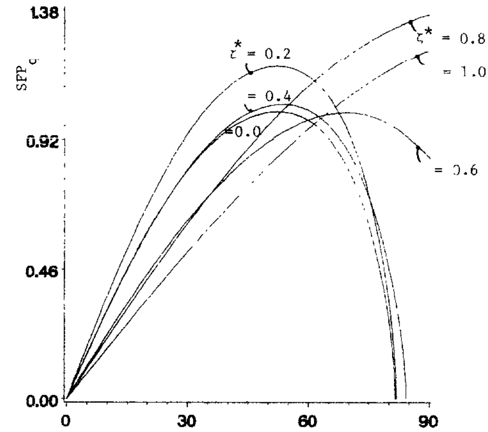

FIG. 7(b). Angular distributions of the skin friction parameter (SFP_q) for a constant heat flux sphere covering the entire free–forced convection range ($Pr = 0.7$, $BP = 1$, $MP = 0$, $Z = 1$).

and

$$u/[(\alpha/R)Ra^{*2/5}] = \sigma^{2/5}F'(\xi,\eta)(u_e/u_\infty)/\zeta^{*2}$$
$$\text{for } q_w = \text{const.} \tag{40b}$$

Figure 2 shows the dimensionless profiles $F'(\eta)$ on a sphere at $\phi = 60^\circ$ covering the entire range of free–forced convection heat transfer. The evolution from pure free convection ($\zeta = 1.0$) to pure forced convection ($\zeta = 0$) is uniformly shown. An increase in body spin (i.e. $BP > 1$) leads to a decrease in momentum boundary-layer thickness and larger velocities. To illustrate how the buoyancy force and the centrifugal force affect the boundary-layer flow field, representative velocity profiles are shown in Fig. 3 for a heated isothermal sphere. It is noted that the traditional coordinate $\eta^* = Re^{1/2}y/R$ has been used. For aiding flow (i.e. $Z = 1$), the velocity gradient at the wall increases as the buoyancy force or the centrifugal force is increased. This is accompanied by higher boundary-layer velocities which may exceed the local free-stream velocity. Figure 4 depicts velocity profiles at different locations along the sphere for opposing flow (i.e. $Z = -1$). Forced convection supported by body rotation ($BP = 1.0$) is retarded by the buoyancy force ($\zeta = 0.5$) which acts like an adverse pressure gradient. It can be seen that for this particular set of system parameters, flow separation may occur for $\xi > 1.368$. The strong effect of the fluid Prandtl number on the magnitude of the dimensionless velocity and the boundary-layer thickness is given in Fig. 5 for the case of natural convection for a sphere.

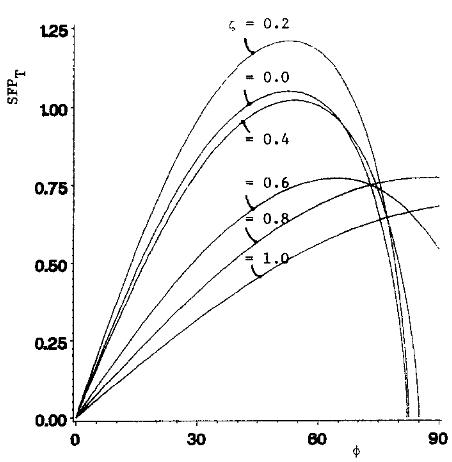

FIG. 7(a). Angular distributions of the skin friction parameter (SFP_T) for an isothermal sphere covering the entire free–forced convection range ($Pr = 0.7$, $BP = 1$, $MP = 0$, $Z = 1$).

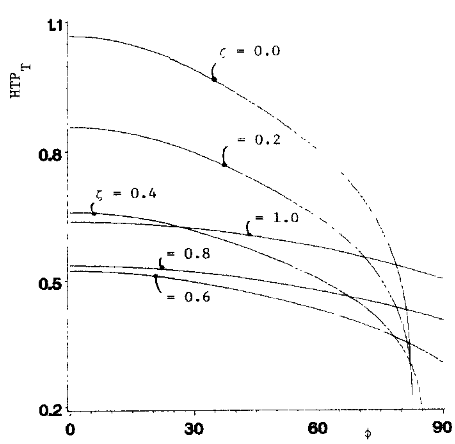

FIG. 8(a). Angular distributions of the heat transfer parameter (HTP_T) for an isothermal sphere covering the entire free–forced convection range ($Pr = 0.7$, $BP = 1$, $MP = 0$, $Z = 1$).

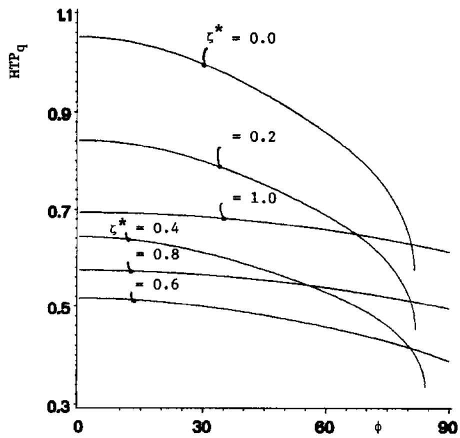

FIG. 8(b). Angular distributions of the heat transfer parameter (HTP_q) for a constant heat flux sphere covering the entire free–forced convection range ($Pr = 0.7$, $BP = 1$, $MP = 0$, $Z = 1$).

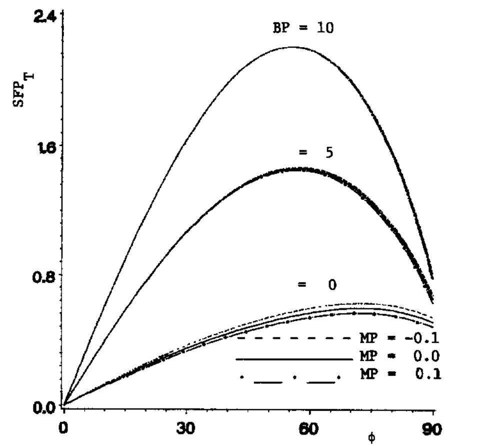

FIG. 9(b). Effects of mass transfer parameter and rotation parameter on the skin friction parameter SFP_T ($\zeta = 0.6$, $Pr = 0.7$, $Z = 1$).

Representative temperature profiles within the thermal boundary layer at $\phi = 60°$ are shown in Fig. 6 for the entire range of free–forced convection heat transfer. It is evident that the dimensionless temperature gradient at the wall, $[\theta'(\zeta)]_w \sim Nu(\zeta)$, does not decrease monotonously with increasing buoyancy force. The reason is that θ' decreases in the forced-convection dominated regime since $\eta \sim (1-\zeta)^{-1}$ and then θ' increases when the buoyancy force becomes dominant because $\eta \sim \zeta^{-1}$ in the free-convection dominated regime. It has to be noted that the temperature profiles cannot be plotted for the entire mixed convection range, $0 \leqslant \zeta \leqslant 1$, when the conventional coordinate $\eta^* = Re^{1/2}y/R$ is being used. With higher body spin ($BP > 1.0$), $\theta'(\eta = 0)$ becomes steeper, i.e. rotation enhances heat transfer.

4.3. *Effects of system parameters on local skin friction and Nusselt number distributions*

Figures 7(a) and (b) show the angular distribution of the skin friction parameter (*SFP*) for a rotating sphere with T_w = const. and q_w = const., respectively. Proper selection of a reference velocity u (cf. equations (23) and (35)) allows the simulation of $SFP(\phi)$ for the entire mixed convection parameter range. Clearly, the buoyancy force helps to delay flow separation. The trend of $SFP(\phi)$ is very similar for both thermal boundary conditions. The same is true for the local heat transfer parameter $HTP(\phi)$ depicted in Figs. 8(a) and (b). For a given mixed convection parameter value, the constant wall heat flux case generates higher *SFG* and *HTP* values than the isothermal wall case and the differences diminish for small angles as ζ

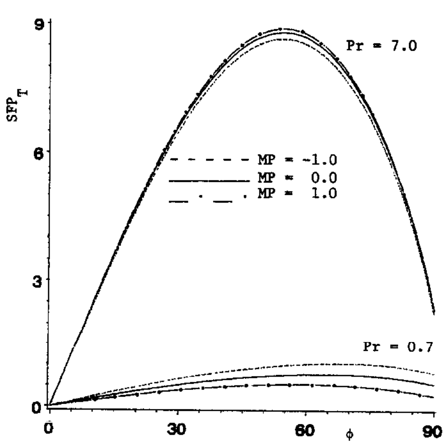

FIG. 9(a). Effects of mass transfer parameter and Prandtl number on the skin friction parameter SFP_T ($\zeta = 0.6$, $BP = 1$, $Z = 1$).

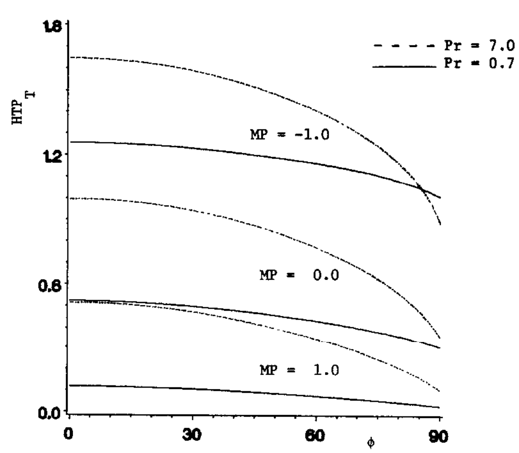

FIG. 10(a). Effects of mass transfer parameter and Prandtl number on the local heat transfer parameter HTP_T ($\zeta = 0.6$, $BP = 1$, $Z = 1$).

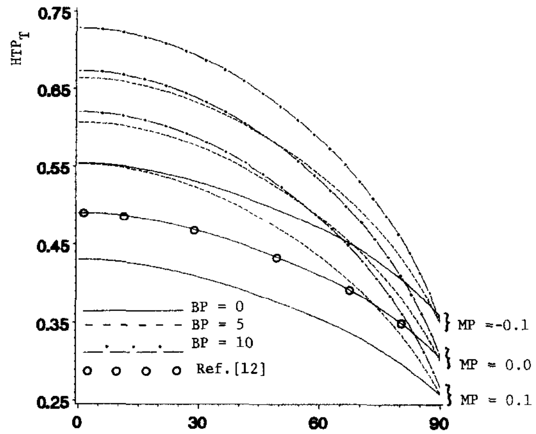

FIG. 10(b). Effects of mass transfer parameter and rotation parameter on the local heat transfer parameter HTP_T ($\zeta = 0.6$, $Pr = 0.7$, $Z = 1$).

approaches zero. Another general observation is that with a stronger influence of the buoyancy force, the trends in *SFP*- and *HTP*-values are reversed for $\phi \leqslant 60°$. For example, $HTP(\zeta)$ decreases on the front part of the sphere until $\zeta \approx 0.6$ and then, in the free-convection dominated regime, $HTP(\zeta)$ increases.

The effects of the mass transfer parameter, *MP*, the rotation parameter, *BP*, and the Prandtl number, *Pr*, on the local skin friction coefficient and the local Nusselt number are shown in Figs. 9(a), (b) and 10(a), (b). Considering a fixed value, $\zeta = 0.6$, the influence of wall mass transfer on *SFP* is more noticeable at low Prandtl numbers. Actually, the Prandtl number may reverse the role of fluid injection and suction (cf. Fig. 9(a)). At $Pr = 0.7$, fluid withdrawal increases and blowing decreases the skin friction coefficient while the effect of *MP* diminishes as *BP* increases (cf. Fig. 9(b)). It is evident from Fig. 10(a) that suction increases the local Nusselt number, $Nu \sim \theta'$ ($\eta = 0$), because the temperature gradient at the wall is greater when cooler fluid is drawn towards the heated isothermal surface. Conversely, injection of warm fluid decreases the Nusselt number and this effect is more pronounced at higher Prandtl numbers. However, one has to keep in mind that $\lambda = \lambda(Pr)$ so that, for example in this case, $\lambda(Pr = 7.0) \approx 2.44$ $\lambda(Pr = 0.7)$. In general, the heat transfer parameter, HTP_T, decreases with angular position. While $HTP_T(\phi)$ is larger with high body rotation as discussed earlier, it also declines more rapidly along the sphere's surface at higher centrifugal forces. This is shown in Fig. 10(b) together with the fluid suction/injection effect.

5. CONCLUSIONS

A generalized analysis of laminar mixed convection heat and surface mass transfer between Newtonian fluids and rotating permeable bodies of arbitrary axisymmetric shape has been presented. Two new mixed thermal convection parameters, ζ and ζ^*, have been introduced to replace the conventional Richardson numbers, Gr/Re^2 and $Gr/Re^{5/2}$, for the isothermal wall case and the constant wall heat flux case, respectively. Furthermore, appropriate coordinate transformations yielded computationally efficient numerical solutions which are uniformly valid over the entire range from pure forced convection to pure free convection, i.e. $0 \leqslant \zeta$ or $\zeta^* \leqslant 1$. The validated computer simulation model has been applied to the case of mixed thermal convection past a rotating sphere with optional fluid suction or injection, surface heating or cooling mode, and thermal boundary condition T_w = const. or q_w = const. Of particular interest are the effects of fluid Prandtl number, buoyancy force, body rotation, wall mass transfer and type of thermal wall condition on the local skin friction coefficient and on the local Nusselt number.

The results of the parametric sensitivity analyses can be summarized as follows.

(1) Aiding buoyancy force, wall suction, body rotation and high Prandtl number fluids enhance heat transfer.

(2) The separation angle of a heated sphere increases with increasing ζ or ζ^* because the forced-flow assisting buoyancy force generates steep velocity gradients at the wall ($\tau_w \sim \partial u/\partial y$) and helps to delay flow separation.

(3) The impact of blowing/suction on *SFP* is more pronounced at low Prandtl numbers and low body rotation.

(4) The effect of the fluid injection or withdrawal on heat transfer is very significant for high Prandtl number fluids.

(5) Low body spin creates more uniform *HTP* distributions than high rotation.

(6) The constant wall heat flux case generates high *SFP* and *HTP* values than the isothermal surface case; however, the differences diminish for small to moderate angles as ζ and ζ^* approach zero.

Acknowledgement—This work has been supported in part by the Department of Energy, Office of Basic Energy Science; Grant No. DE-FG05-87ER13728.

REFERENCES

1. C. L. Tien and J. Tsuji, Heat transfer by laminar forced flow against a non-isothermal rotating disk, *Int. J. Heat Mass Transfer* **7**, 247–252 (1964).
2. B. T. Chao and R. Greif, Laminar forced convection over rotating bodies, *ASME J. Heat Transfer* **96**, 463–466 (1974).
3. M. H. Lee, D. R. Jeng and K. J. Dewitt, Laminar boundary layer heat transfer over rotating bodies in forced flow, *ASME J. Heat Transfer* **100**, 496–502 (1978).
4. F. S. Lien, C. K. Chen and J. W. Cleaver, Mixed and free convection over a rotating sphere with blowing and suction, *ASME J. Heat Transfer* **108**, 398–404 (1986).
5. C. Kleinstreuer and T. Y. Wang, Heat transfer between rotating spheres and flowing power-law fluids with suc-

tion and injection, *Int. J. Heat Fluid Flow* **9**, 328–333 (1988).
6. H. T. Lin and C. C. Chen, Mixed convection on vertical plate for fluids of any Prandtl number, *Wärme- und Stoffübertr.* **22**, 159–168 (1988).
7. S. L. Lee, T. S. Chen and B. F. Armaly, Mixed convection along vertical cylinders and needles with uniform heat flux, *ASME J. Heat Transfer* **109**, 711–716 (1987).
8. T.-Y. Wang and C. Kleinstreuer, General analysis of steady laminar mixed convection heat transfer on vertical slender cylinders, *ASME J. Heat Transfer* (1989), in press.
9. C. Kleinstreuer, *Engineering Fluid Dynamics—An Interdisciplinary Systems Approach.* Springer, New York (to be published).
10. N. Frössling (1958) in F. M. White, *Viscous Fluid Flow.* McGraw-Hill, New York (1974).
11. T. Cebeci and P. Bradshaw, *Momentum Transfer in Boundary Layers.* Hemisphere, Washington, DC (1977).
12. T. S. Chen and A. Mucoglu, Analysis of mixed forced and free convection about a sphere, *Int. J. Heat Mass Transfer* **20**, 867–875 (1977).

CONVECTION MIXTE SUR DES CORPS TOURNANTS AVEC SOUFFLAGE OU ASPIRATION

Résumé—On élargit et on clarifie l'analyse de la couche limite non affine pour la convection thermique mixte laminaire sur un corps axisymétrique. On étudie les profils de vitesse et de température dans les couches limites attachées pour le domaine complet depuis la convection forcée pure jusqu'à la convection naturelle pure. Le modèle traité sur ordinateur est appliqué avec succès au cas de la convection mixte pour des fluides à nombre de Prandtl quelconque, autour d'une sphère avec optionnellement, rotation du solide, aspiration ou soufflage du fluide, chauffage ou refroidissement de la surface et une condition pariétale de température ou de flux uniforme.

GEMISCHTE KONVEKTION ÜBER ROTIERENDE KÖRPER MIT AUSBLASUNG UND ABSAUGUNG

Zusammenfassung—Die Grenzschichtanalyse des stationären laminaren Wärmeübergangs mit gemischter Konvektion an axial-symmetrischen Körpern wird erweitert und vereinheitlicht. Über den gesamten Bereich von reiner Zwangskonvektion bis zu völlig freier Konvektion werden Geschwindigkeitsprofile und Temperaturverteilung in den anliegenden Grenzschichten untersucht. Ein validiertes Computersimulationsmodell wird erfolgreich angewandt auf den Fall gemischter thermischer Konvektion von Fluiden beliebiger Prandtl-Zahl hinter einer Kugel mit wahlweise Körperrotation, Absaugen oder Ausblasen von Fluid, Oberflächenheizung oder -kühlung, isothermer Randbedingung oder konstanter Wärmestromdichte.

СМЕШАННАЯ КОНВЕКЦИЯ НАД ВРАЩАЮЩИМИСЯ ТЕЛАМИ ПРИ ВДУВЕ И ОТСОСЕ

Аннотация—Расширен и унифицирован неавтомодельный анализ в приближении пограничного слоя для стационарного теплопереноса от осесимметричного тела в условиях ламинарной смешанной конвекции. Профили скорости и температуры в пограничных слоях исследуются для всего диапазона — от чисто вынужденной до чисто свободной конвекции. Обоснована модель для численного исследования, которая успешно применена для случая смешанной тепловой конвекции жидкостей с произвольным числом Прандтля за сферой при возможном вращении тела, отсосе или вдуве жидкости, нагреве или охлаждении поверхности, в условиях изотермических стенок или постоянного теплового потока на стенках.